Original Article

MOLECULAR METABOLISM

Ube2i deletion in adipocytes causes lipoatrophy in mice

Aaron R. Cox [1,2], Natasha Chernis [1,2], Kang Ho Kim [3], Peter M. Masschelin [1,2,3], Pradip K. Saha [1,2], Shawn M. Briley [3,4], Robert Sharp [1,2], Xin Li [1,2], Jessica B. Felix [1,2,3], Zheng Sun [1,2,3], David D. Moore [3], Stephanie A. Pangas [3,5], Sean M. Hartig [1,2,3,*]

ABSTRACT

Objective: White adipose tissue (WAT) expansion regulates energy balance and overall metabolic homeostasis. The absence or loss of WAT occurring through lipodystrophy and lipoatrophy contributes to the development of hepatic steatosis and insulin resistance. We previously demonstrated that sole small ubiquitin-like modifier (SUMO) E2-conjugating enzyme *Ube2i* represses human adipocyte differentiation. The role of *Ube2i* during WAT development remains unknown.

Methods: To determine how *Ube2i* impacts body composition and energy balance, we generated adipocyte-specific *Ube2i* knockout mice (*Ube2i*$^{a\text{-}KO}$). CRISPR/Cas9 gene editing inserted loxP sites flanking exons 3 and 4 at the *Ube2i* locus. Subsequent genetic crosses to Adipoq-Cre transgenic mice allowed deletion of *Ube2i* in white and brown adipocytes. We measured multiple metabolic endpoints that describe energy balance and carbohydrate metabolism in *Ube2i*$^{a\text{-}KO}$ and littermate controls during postnatal growth.

Results: Surprisingly, *Ube2i*$^{a\text{-}KO}$ mice developed hyperinsulinemia and hepatic steatosis. Global energy balance defects emerged from dysfunctional WAT marked by pronounced local inflammation, loss of serum adipokines, hepatomegaly, and near absence of major adipose tissue depots. We observed progressive lipoatrophy that commences in the early adolescent period.

Conclusions: Our results demonstrate that *Ube2i* expression in mature adipocytes allows WAT expansion during postnatal growth. Deletion of *Ube2i* in fat cells compromises and diminishes adipocyte function that induces WAT inflammation and ectopic lipid accumulation in the liver. Our findings reveal an indispensable role for *Ube2i* during white adipocyte expansion and endocrine control of energy balance.

Keywords *Ube2i*; Lipodystrophy; Adipose tissue; Lipid metabolism

1. INTRODUCTION

White adipocytes sequester lipids and protect peripheral metabolic tissues from ectopic lipid accumulation. Consequently, the failure of integral lipid metabolism responses and reduced adipose tissue expandability during chronic states of positive energy balance contribute to the development of insulin resistance, obesity, and fatty liver disease [1]. Similar metabolic abnormalities develop in patients with lipodystrophy where a lack of adipose tissue does not allow storage of surfeit energy as lipids, leading to insulin resistance, hepatic steatosis, and dyslipidemia [2]. Therefore, healthy adipose tissue development mediates key aspects of metabolic homeostasis.

Physiologic WAT expansion occurs through both increased adipocyte size (hypertrophy) and number (hyperplasia). White adipocyte differentiation requires a cascade of transcription factors that activate PPARγ, the master regulator of adipocyte differentiation [3]. Adipocyte differentiation requires PPARγ [4] to partner with distinct transcriptional co-regulators that coordinate brown and white adipocyte-specific gene expression [5,6]. Gene deletion or tissue-specific disruption of PPARγ impairs adipogenesis and results in severe lipodystrophy [4,7–9]. The mechanisms that enable adipose tissue development have broad basic implications for understanding energy balance disorders.

We previously showed *Ube2i* depletion in human subcutaneous preadipocytes accelerated fat cell differentiation [10]. In this study, we generated an adipocyte-specific *Ube2i* knockout (*Ube2i*$^{a\text{-}KO}$) mouse to investigate how *Ube2i* regulates whole-body energy balance. Surprisingly, WAT mass failed to expand in male and female *Ube2i*$^{a\text{-}KO}$ mice. Progressive lipoatrophy and compromised adipocyte function likely provoked WAT inflammation and ectopic lipid accumulation leading to insulin resistance, impaired brown adipose tissue (BAT) function, and intolerance to cold temperatures. Taken together, our findings reveal critical roles for *Ube2i* in adipocyte function and expansion.

[1]Division of Diabetes, Endocrinology, and Metabolism, Baylor College of Medicine, Houston, TX, USA [2]Department of Medicine, Baylor College of Medicine, Houston, TX, USA [3]Department of Molecular and Cellular Biology, Baylor College of Medicine, Houston, TX, USA [4]Biochemistry and Molecular Biology, Baylor College of Medicine, Houston, TX, USA [5]Department of Pathology and Immunology, Baylor College of Medicine, Houston, TX, USA

*Corresponding author. One Baylor Plaza, MS: BCM185, Houston, TX, 77019, USA. E-mail: hartig@bcm.edu (S.M. Hartig).

Received January 15, 2021 • Revision received March 11, 2021 • Accepted March 22, 2021 • Available online 24 March 2021

https://doi.org/10.1016/j.molmet.2021.101221

Abbreviations

a-KO	adipocyte-specific knockout
BAT	brown adipose tissue
CGL	congenital generalized lipodystrophy
CLAMS	Comprehensive Lab Animal Monitoring System
CRISPR	Clustered Regularly Interspace Short Palindromic Repeats
DAPI	4′,6-diamidino-2-phenylindole
ELISA	enzyme linked immunosorbent assay
FGF21	fibroblast growth factor 21
FPLD	familial partial lipodystrophy
GFP	green fluorescent protein
gWAT	gonadal white adipose tissue
H/E	Hematoxylin and Eosin
IP	intraperitoneal
iWAT	inguinal white adipose tissue
loxP	locus of X-over P1
PBS	Phosphate Buffered Saline
PPARγ	Peroxisome proliferator-activated receptor gamma
RER	respiratory exchange ratio
sgRNA	single guide RNA
lssDNA	long single-stranded oligodeoxynucleotide donor
SUMO	Small Ubiquitin-like Modifier
SVF	stromal vascular fraction
TG	triglyceride
Ube2i	Ubiquitin conjugating enzyme E2 I
WAT	White adipose tissue

2. METHODS

2.1. Animals

All procedures with animals were approved by the Institutional Animal Care and Use Committee of Baylor College of Medicine (animal protocol AN-6411). Experimental animals received humane care according to criteria in the "Guide for the Care and Use of Laboratory Animals" (8th edition, revised 2011). Experimental animals were housed (no more than four per cage) in a barrier-specific pathogen-free animal facility with 12-h dark—light cycle and free access to water and normal chow (Harlan Laboratories 2920X). All experiments were conducted using littermate-controlled male and female mice maintained on a C57BL/6J background. At the end of experiments, mice were euthanized by cervical dislocation while under isoflurane anesthesia. After euthanasia, tissues were collected, flash-frozen in liquid N_2, and stored at −80 °C until use. All experiments adhered to ARRIVE Guidelines.

2.2. Generation of a conditional *Ube2i* allele

Ube2i$^{fl/fl}$ mice were generated by the Genetically Engineered Rodent Models Core at BCM using previously established methods [11]. We employed Cas9-initiated homology-driven repair (HDR) using a pair of single guide RNAs (sgRNAs) coupled with a long single-stranded oligodeoxynucleotide donor (lssDNA) template harboring short homology arms and loxP-flanked exons. The sgRNAs and the lssDNA donor were used to insert loxP sites 5′ and 3′ of exons 3 and 4 of the mouse *Ube2i* gene, respectively. Sequences of the sgRNAs and lssDNA donor are included in Supplemental File 1. To minimize the probability of off-target events, only sgRNAs predicted to have off-target sites with three mismatches or more were used to target Cas9 endonuclease activity to intronic sequences flanking exon 3 and 4. Two hundred C57BL/6NJ pronuclear-stage zygotes were co-injected with Cas9 mRNA, sgRNAs, and lssDNA [11]. Following micro-injection, zygotes were transferred into pseudopregnant ICR recipient females at approximately 25—32 zygotes per recipient. Sanger sequencing of cloned loxP sites and founder line genotyping from mouse genomic DNA confirmed loxP insertions and sequence fidelity. Progeny generated from putative founders were also sequence-confirmed for the fidelity of the loxP sequences and floxed exons. The targeted sequence and annotated primer locations are included in Supplemental File 2 (GenBank). *Ube2i*$^{fl/fl}$ mice were crossed with Adipoq-Cre (Jackson Laboratory #028020) to generate adipocyte-specific *Ube2i* knockout (*Ube2i*$^{a\text{-}KO}$) and littermate controls (*Ube2i*$^{fl/fl}$). *Ube2i*$^{fl/fl}$ mice were crossed with CAG-CreER™ (Jackson Laboratory #004682) to generate tamoxifen inducible *Ube2i* gene deletion. *Ube2i*$^{fl/fl}$ are distributed upon request.

2.3. Genotyping

DNA extracted from mouse ear clips was used in PCR reactions with primers designed to detect the 5′ (P1 - AGGTAGGGGTGGCTTAGAGG, P2 - GGTTCATTGTGCCATCAGGG) and 3′ (P3 - CAAGTCCCAGGGTAGATGCG, P4 - CAGCTCAGACCTGGCCTTAC) loxP sequences and run on agarose gels. Cre transgenic mice were genotyped according to protocols provided by the Jackson Laboratory.

2.4. Antibodies and western blotting

Tissue and whole cell lysates were prepared in Protein Extraction Reagent (Thermo Fisher) supplemented with Halt Protease and Phosphatase Inhibitor Cocktail (Thermo Fisher). Immunoblotting was performed with lysates run on 4—12% Bis-Tris NuPage gels (Life Technologies) and transferred onto Immobilon-P Transfer Membranes (Millipore) followed by antibody incubation. Immunoreactive bands were visualized by chemiluminescence. The following antibodies were used for immunoblotting: α-HSP90 (Cell Signaling #4877), α-UBE2I (Cell Signaling #4786), α-ADIPOQ (Genetex #GTX112777), α-PPARγ (Cell Signaling #2443), α-Caspase-8 (Cell Signaling #4790), and α-Cleaved Caspase-8 (Cell Signaling #8592).

2.5. Cell culture

To validate Cre-inducible deletion of *Ube2i*, fibroblasts were isolated from the inguinal white adipose tissue (iWAT) stromal vascular fraction (SVF) of *Ube2i*$^{fl/fl}$ mice. iWAT depots were digested in phosphate buffered saline (PBS) containing collagenase D (Roche, 1.5 U/mL) and dispase II (Sigma, 2.4 U/mL) supplemented with 10 mM $CaCl_2$ at 37 °C for 45 min. The primary cells were filtered twice through 70 μm strainers and centrifuged to collect the SVF. For adenovirus transduction, SVF cells were incubated with adenoviral Cre recombinase or green fluorescent protein (GFP) in DMEM/F12 medium containing Glutamax (ThermoFisher) and 10% fetal bovine serum (FBS) for 24 h. After replacing the medium once, cells were cultured for 48 h before lysate preparation. Adenoviruses expressing Cre recombinase or GFP were provided by the BCM Gene Vector Core. Similarly, iWAT SVF cells were isolated from *CAG-Cre*^{ER};*Ube2i*$^{fl/fl}$ mice, treated with 1 μM 4-hydroxytamoxifen for 48 h followed by differentiation for eight days.

2.6. Indirect calorimetry

Ube2i$^{a\text{-}KO}$ and littermate controls (*Ube2i*$^{fl/fl}$) were maintained on normal chow and housed at room temperature in Comprehensive Lab Animal Monitoring System (CLAMS) home cages (Columbus Instruments). Oxygen consumption, CO_2 emission, energy expenditure, food and water intake, and activity were measured for six days (BCM Mouse Metabolic and Phenotyping Core). Mouse body weight was recorded,

and body composition examined by magnetic resonance imaging (Echo Medical Systems) prior to indirect calorimetry. Statistical analysis of energy balance was performed by ANCOVA with lean body mass as a co-variate using the CalR web-based tool [12].

2.7. Glucose and insulin tolerance tests

To determine glucose tolerance, mice were fasted for 16 h and glucose was administered (1.5 g/kg body weight) by intraperitoneal (IP) injection. To determine insulin tolerance, mice were fasted 4 h prior to insulin intraperitoneal injection (1.5 U/kg body weight). Blood glucose levels were measured by a handheld glucometer. Serum was collected after fasting and during glucose tolerance tests for insulin quantification.

2.8. ELISAs and lipid assays

Fed serum levels were used to measure insulin (#EZRMI-13K; Millipore), leptin (#90030; Crystal Chem), adiponectin (#KMP0041; Thermo Fisher), and free fatty acids (#sfa-1; ZenBio), and FGF21 (#MF2100; R&D Systems). Insulin levels during glucose tolerance tests were also measured by ELISA (Millipore). Hepatic triglyceride (TG) content was quantified by Thermo Fisher Scientific Triglycerides Reagent (#TR22421) and normalized per gram of liver tissue.

2.9. Histology

Formalin-fixed paraffin-embedded adipose and liver tissue sections were stained with hematoxylin and eosin (H/E) by the BCM Human Tissue Acquisition and Pathology Core. Images were captured using a Nikon Ci-L Brightfield microscope.

2.10. Fluorescence microscopy

Following differentiation, media was aspirated and 4% formaldehyde (Electron Microscopy Sciences) in PBS was immediately added for 30 min at room temperature. Excess paraformaldehyde was quenched with 100 mM ammonium chloride. Non-specific antibody binding was blocked by pre-incubating for 30 min in 2% bovine serum albumin in PBS/0.01% saponin (which was also used as an antibody diluent) at room temperature. Anti-perilipin antibody (GP-29, Progen) was diluted at a 1:1000 concentration in antibody diluent and incubated overnight at 4 °C. Subsequently, coverslips were washed with PBS and incubated with secondary antibodies for 1 h at room temperature. AlexaFluor 647-conjugated anti-guinea pig secondary antibodies (Thermo Fisher) were used. Coverslips were then washed 3 times and incubated LipidTOX green (1:1000, Thermo Fisher) and DAPI (10 μg/mL) in PBS for 45 min at room temperature. Slides were mounted with SlowFade Gold (ThermoFisher). Imaging was performed with the DeltaVision Core Image Restoration Microscope (GE Healthcare).

2.11. qPCR

Total RNA was extracted using the Direct-zol RNA MiniPrep kit (Zymo Research). cDNA was synthesized using iScript (Bio-Rad). Relative mRNA expression was measured with SsoAdvanced Universal Probes Supermix reactions read out with a QuantStudio 3 real-time PCR system (Applied Biosystems). TATA-box binding protein (*Tbp*) was the invariant control. Roche Universal Probe Gene Expression Assays were used as previously described [13].

2.12. Cold tolerance test

Six-month old male $Ube2i^{fl/fl}$ and $Ube2i^{a\text{-}KO}$ mice were individually housed with water and exposed to cold temperature (4 °C) for 2.5 h. A temperature probe was placed subcutaneously on top of the intrascapular BAT two days prior to the cold tolerance test. Temperature recordings were measured in duplicate at room temperature (time = 0) and during cold exposure every 30 min.

2.13. Statistical analyses

Statistical significance was assessed by unpaired Student's t-test with a primary threshold for statistical significance set at $p < 0.05$. For gene expression data, statistical significance was assessed by multiple unpaired t-tests with a q-value < 0.05. Statistical analysis of energy balance was performed by ANCOVA with lean body mass as a co-variate and cumulative food intake by standard ANOVA using the CalR web-based tool [12]. All data are presented as mean ± standard error of the mean (SEM), unless otherwise stated.

3. RESULTS

3.1. Generation of conditional *Ube2i* knockout mice

Ube2i is expressed ubiquitously across all mouse tissues [14] and knockout strategies cause lethality and sterility [14–17]. To this end, we used CRISPR/Cas9 gene editing to generate a conditional *Ube2i* allele ($Ube2i^{fl/fl}$) to explore tissue-specific roles for *Ube2i*. LoxP sites flanking exons 3 and 4 of the *Ube2i* locus were introduced by homology-directed repair (Figure 1A) and the *in vivo* presence of loxP sites in the targeted regions was confirmed by genotyping of potential founder mice (Figure 1B). We verified that the loxP sites targeted the *Ube2i* locus by transfecting $Ube2i^{fl/fl}$ iWAT-derived fibroblasts with adenovirus expressing Cre recombinase. Immunoblot analysis of whole cell lysates demonstrated near total deletion of UBE2I protein levels following Cre recombination compared to adenovirus GFP transductions (Figure 1C). To determine the cell autonomous effects of *Ube2i* deletion in adipocytes, CAG-Cre^{ER} mice were crossed with $Ube2i^{fl/fl}$ mice and we isolated iWAT SVF cells for *in vitro* differentiation. Tamoxifen treatment knocked out UBE2I only in cells expressing *CAG-Cre;*$Ube2i^{fl/fl}$, regardless of differentiation status (Figure 1D). Although we observed efficient UBE2I protein depletion, inducible knockout of *Ube2i* left representative adipocyte differentiation genes unaffected (Figure 1E). However, we observed a dramatic increase in several brown/beige adipocyte marker genes, including *Ucp1*, *Prdm16*, *Cidea*, and *Cited1*, consistent with observations from human subcutaneous adipocytes [10]. Although Western blot and qPCR showed the expression of mature adipocyte markers, we observed fewer lipid droplets in *Ube2i* knockout adipocytes (Figure 1F). We also observed higher cleaved Caspase-8 levels indicative of dying adipocytes (Figure 1G), which suggests an important role for UBE2I in adipocyte survival.

To specifically study the *in vivo* effects of *Ube2i* deletion in mature fat cells, we generated adipose-specific *Ube2i* knockout mice ($Ube2i^{a\text{-}KO}$) by crossing $Ube2i^{fl/fl}$ animals with Adipoq-Cre transgenic mice (Figure 1H). Reproductive fitness and female nursing were unaffected by $Ube2i^{a\text{-}KO}$ and all pups were viable and born at the expected Mendelian ratio. PCR analysis demonstrated Cre recombination of the *Ube2i* locus generated a deletion product (red arrow) in the gonadal WAT (gWAT) from $Ube2i^{a\text{-}KO}$ mice that was absent in $Ube2i^{fl/fl}$ controls (Figure 1I). The full length, unrecombined product (green arrow) was also detected in $Ube2i^{a\text{-}KO}$, but at lower levels than control, suggesting contributions of Cre-negative cells in the SVF to the PCR product. Similarly, UBE2I protein was reduced in iWAT and brown adipose tissue (BAT) compared to $Ube2i^{fl/fl}$ controls (Figure 1J).

3.2. Adipocyte-specific *Ube2i* deletion impairs WAT expansion during postnatal growth

To determine the impact of adipocyte *Ube2i* loss in mice, we examined body weight (Figure 2A) and WAT mass (Figure 2B) at necropsy from

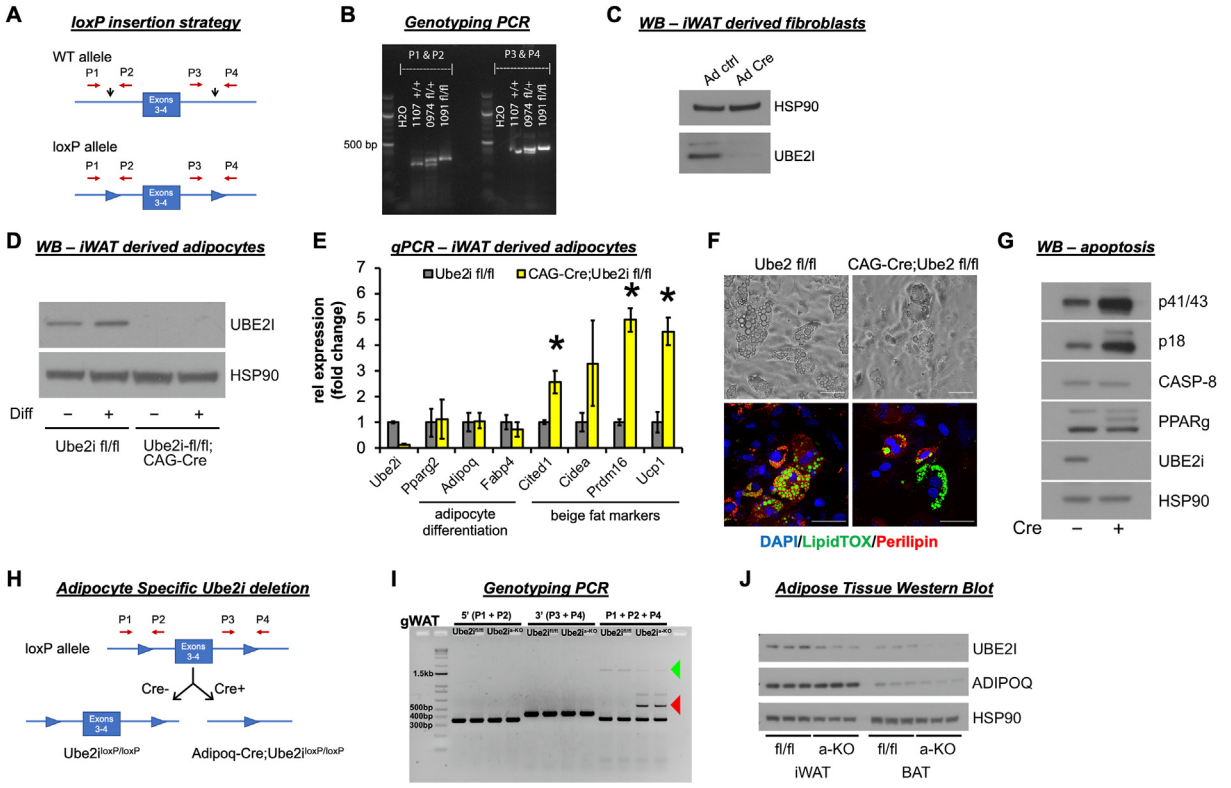

Figure 1: Generation of conditional *Ube2i* gene deletion mice. (A) *Ube2i*$^{fl/fl}$ mice were generated using CRISPR/Cas9 gene editing. Exons 3 and 4 of the *Ube2i* (*Ubc9*) gene were targeted by sgRNAs designed complementary to intronic sequences flanking the exons, then loxP sequences were introduced by DNA donor oligonucleotides. LoxP sites were inserted before exon 3 and after exon 4 (black arrows). Primers detect the 5' (P1, P2) and 3' (P3, P4) loxP sequences. **(B)** PCR analyses of floxed alleles at the targeted loci in genomic DNA extracted from ear clips of wild-type (+/+), fl/+, and fl/fl mice. PCR products were run on agarose gels with expected band sizes for P1—P2: wild-type (+) 319 bp and loxP allele (fl) 353 bp and P3—P4: wild-type (+) 427 bp and loxP allele (fl) 461 bp. The image shows a wild-type control #1107 +/+, founder heterozygous mouse #974 fl/+, and homozygous F2 offspring #1091 fl/fl. **(C)** Western blot analysis of UBE2I expression in inguinal WAT (iWAT) derived fibroblasts from *Ube2i*$^{fl/fl}$ mice after transduction with adenoviral GFP or Cre. To determine cell autonomous effects of *Ube2i* deletion in adipocytes, tamoxifen inducible Cre-expressing mice (*CAG-Cre*) were crossed with *Ube2i*$^{fl/fl}$ mice. iWAT SVF cells were isolated from *CAG-Cre;Ube2i*$^{fl/fl}$ and *Ube2i*$^{fl/fl}$ control mice. All cells were treated with tamoxifen to induce Cre recombination followed by adipocyte differentiation (diff) for eight days. **(D)** Western blot analysis and **(E)** relative gene expression by qPCR were performed to assess Ube2i depletion, adipocyte maturation, and beige fat cell markers. Gray = *Ube2i*$^{fl/fl}$, yellow = *CAG-Cre;Ube2i*$^{fl/fl}$. Data are presented as mean +/− SEM, *p < 0.05. **(F)** Brightfield and fluorescent images of differentiated *Ube2i*$^{fl/fl}$ and *CAG-Cre;Ube2i*$^{fl/fl}$ cells stained for lipids (green, LipidTOX), perilipin (red), and nuclei (blue, DAPI). Scale bars 50 μm. **(G)** Whole cell lysates from differentiated cells were subjected to Western blot analysis of cleaved (p41/43, p18) and uncleaved Caspase-8. **(H)** Strategy for generating adipocyte-specific *Ube2i* gene deletion. *Ube2i*$^{fl/fl}$ mice were bred with *Adipoq-Cre* mice to generate adipocyte-specific *Ube2i* knockout (*Ube2i*$^{a\text{-}KO}$) and *Ube2i*$^{fl/fl}$ (control) mice. **(I)** To validate gene deletion of *Ube2i*, genomic DNA was extracted from *Ube2i*$^{a\text{-}KO}$ and *Ube2i*$^{fl/fl}$ gonadal WAT (gWAT) samples and PCR products were run on an agarose gel to detect the 5' (P1, P2 primers) and 3' (P3, P4 primers) loxP sequences, as well as a product that spans exons 3—4 (P1+P2+P4; 1597 bp, green arrow) or the deletion product (509 bp, red arrow). **(J)** Western blots of whole tissue lysates from iWAT and BAT of seven-day-old mice were probed for UBE2I and adiponectin (ADIPOQ), and HSP90 served as the invariant loading control.

seven days to six months of age. As expected, *Ube2i*$^{fl/fl}$ control mice exhibited progressive expansion of WAT mass with increasing age (Figure 2B). Conversely, *Ube2i*$^{a\text{-}KO}$ mice failed to expand WAT depots beginning at two months of age and by six months, WAT mass almost completely disappeared relative to *Ube2i*$^{fl/fl}$ controls. Gene expression (Figure 2C) and histological analyses (Figure 2D) of WAT at one month of age revealed similar profiles between *Ube2i*$^{a\text{-}KO}$ and *Ube2i*$^{fl/fl}$ controls, suggesting adipocyte function and morphology are normal prior to impaired WAT expansion. Despite no effects on body weight gain (Figure 2E), magnetic resonance imaging showed reduced fat mass and increased lean mass in six-month-old *Ube2i*$^{a\text{-}KO}$ male and female mice compared to controls (Figure 2F). Further examination of tissue weights at necropsy (Figure 2G) revealed grossly visible reductions (−80%) in iWAT and gWAT depots in male and female *Ube2i*$^{a\text{-}KO}$ mice (Figure 2H). Reduced fat storage in primary WAT depots resulted in significantly higher liver weights associated with gross morphological changes indicative of ectopic lipid accumulation. Similarly, lipid accumulation in BAT was apparent at necropsy, with increased BAT weight detected in female *Ube2i*$^{a\text{-}KO}$ mice. Collectively, these data demonstrate adipocyte-specific deletion of *Ube2i* impairs WAT expansion leading to redistribution of lipid storage.

3.3. Adipocyte-specific *Ube2i* deletion increases WAT inflammation and apoptosis

To assess the morphological changes associated with *Ube2i* knockout in adipose tissues, we performed H/E staining of gWAT and iWAT tissue sections in adult male and female mice. Pronounced immune cell infiltration was observed in gWAT of *Ube2i*$^{a\text{-}KO}$ mice (Figure 3A), distinct from the commonly described crown-like structures typically associated with gWAT [18]. Similarly, we observed dispersed immune cell accumulation amongst stromal cells and large adipocytes in the iWAT of *Ube2i*$^{a\text{-}KO}$ mice. Primary WAT depots from both sexes showed marked stroma invasion and few mature adipocytes. Consistent with reduced numbers of adipocytes, serum levels of adiponectin, leptin,

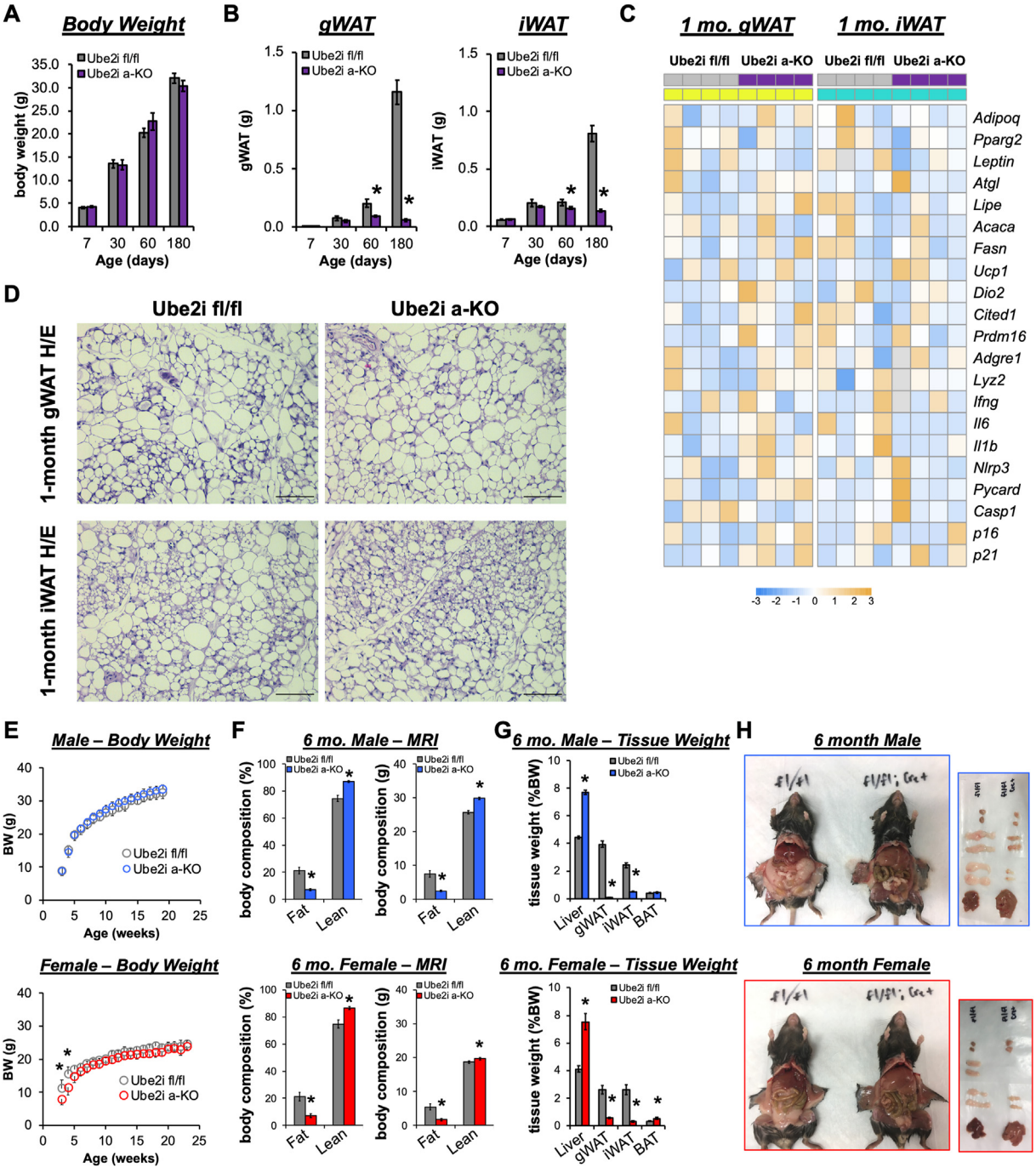

Figure 2: Adipocyte-specific *Ube2i* deletion impairs WAT expansion in male and female mice. (**A**) Body weight and (**B**) WAT weights (g) in combined male and female mice at 7 (n = 5–9), 30 (n = 4/group), 60 (n = 4/group), and 180 (n = 23–24/group) days of age for $Ube2i^{fl/fl}$ (gray) and $Ube2i^{a\text{-}KO}$ (purple) mice. Data are presented as mean +/− SEM; *p < 0.05. (**C**) Relative gene expression by qPCR in gWAT (left, yellow) and iWAT (right, cyan) from $Ube2i^{a\text{-}KO}$ (purple) and $Ube2i^{fl/fl}$ control (gray) mice for adipocyte maturation, lipid metabolism, inflammatory, and senescence genes represented as a heatmap of z-scores. Gray heatmap squares indicate outliers excluded based on Grubbs' test. (**D**) Representative H/E stained gWAT and iWAT sections from one-month-old $Ube2i^{a\text{-}KO}$ and $Ube2i^{fl/fl}$ control mice. Scale bar 100 μm. (**E**) $Ube2i^{a\text{-}KO}$ and $Ube2i^{fl/fl}$ control mice were weighed for up to 23 weeks in males (n = 12–14/group, mean +/− SD) and females (n = 6–8/group, mean +/− SD). (**F**) Assessment of fat and lean mass (% body weight (left) and in grams (right); male n = 11–15/group, female n = 5–7/group). (**G**) Tissue weights (% body weight; male n = 15-16/group, female n = 8/group) at necropsy. (**H**) Corresponding necropsy images from six-month-old $Ube2i^{fl/fl}$ and $Ube2i^{a\text{-}KO}$ mice. Images of excised tissues demonstrate gross morphological increases in liver size, reductions in iWAT and gWAT, and lighter coloring of liver and BAT. (**E**–**H**) Gray = $Ube2i^{fl/fl}$ male and female controls, blue = male $Ube2i^{a\text{-}KO}$, red = female $Ube2i^{a\text{-}KO}$. Data are presented as mean +/− SEM; *p < 0.05.

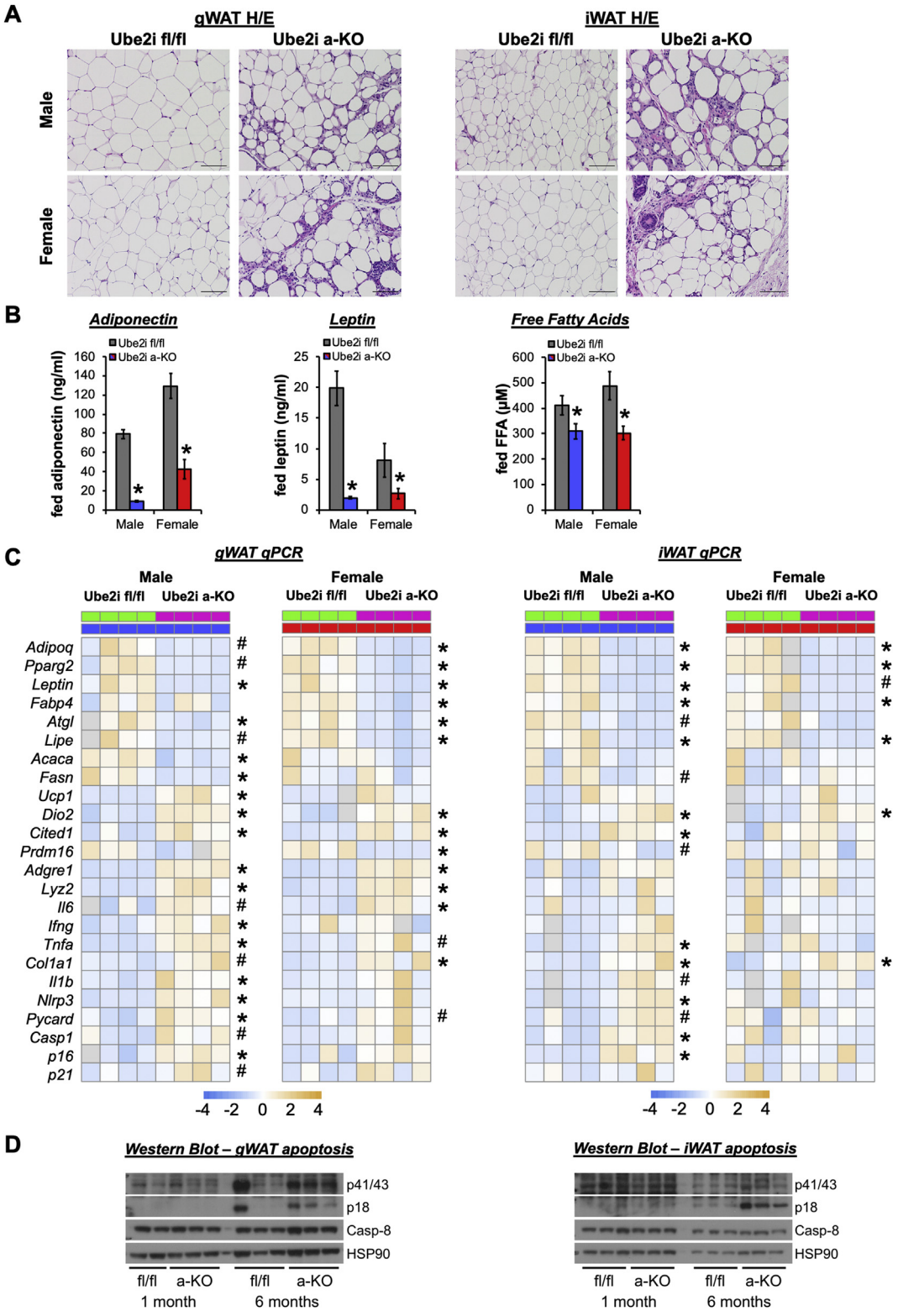

Figure 3: *Ube2i*$^{a\text{-}KO}$ mice display WAT dysfunction with increased inflammation and apoptosis. (A) H/E-stained sections from gWAT and iWAT of male (top row) and female (bottom row) mice show substantial immune and stromal cell infiltration in *Ube2i*$^{a\text{-}KO}$ mice. Scale bar 100 μm. **(B)** Fed serum adiponectin (ng/ml), leptin (ng/ml), and free fatty acids (μM) in male (blue/gray; n = 11–12/group) and female (red/gray; n = 7–9/group) *Ube2i*$^{a\text{-}KO}$ mice compared to *Ube2i*$^{fl/fl}$ controls. Data are presented as mean +/− SEM; *p < 0.05. **(C)** Relative gene expression by qPCR in gWAT (left) and iWAT (right) from male (blue) and female (red) *Ube2i*$^{a\text{-}KO}$ (pink) and *Ube2i*$^{fl/fl}$ control (green) mice for adipocyte maturation, lipid metabolism, inflammatory, and senescence genes represented as a heatmap of z-scores (*p < 0.05, #p < 0.10). Gray heatmap squares indicate outliers excluded based on Grubbs' test. **(D)** Tissue lysates from gWAT (left) and iWAT (right) of *Ube2i*$^{fl/fl}$ and *Ube2i*$^{a\text{-}KO}$ mice were subjected to Western blot analysis of cleaved (p41/43, p18) and uncleaved Caspase-8. All analyses were performed in six-month-old adult mice.

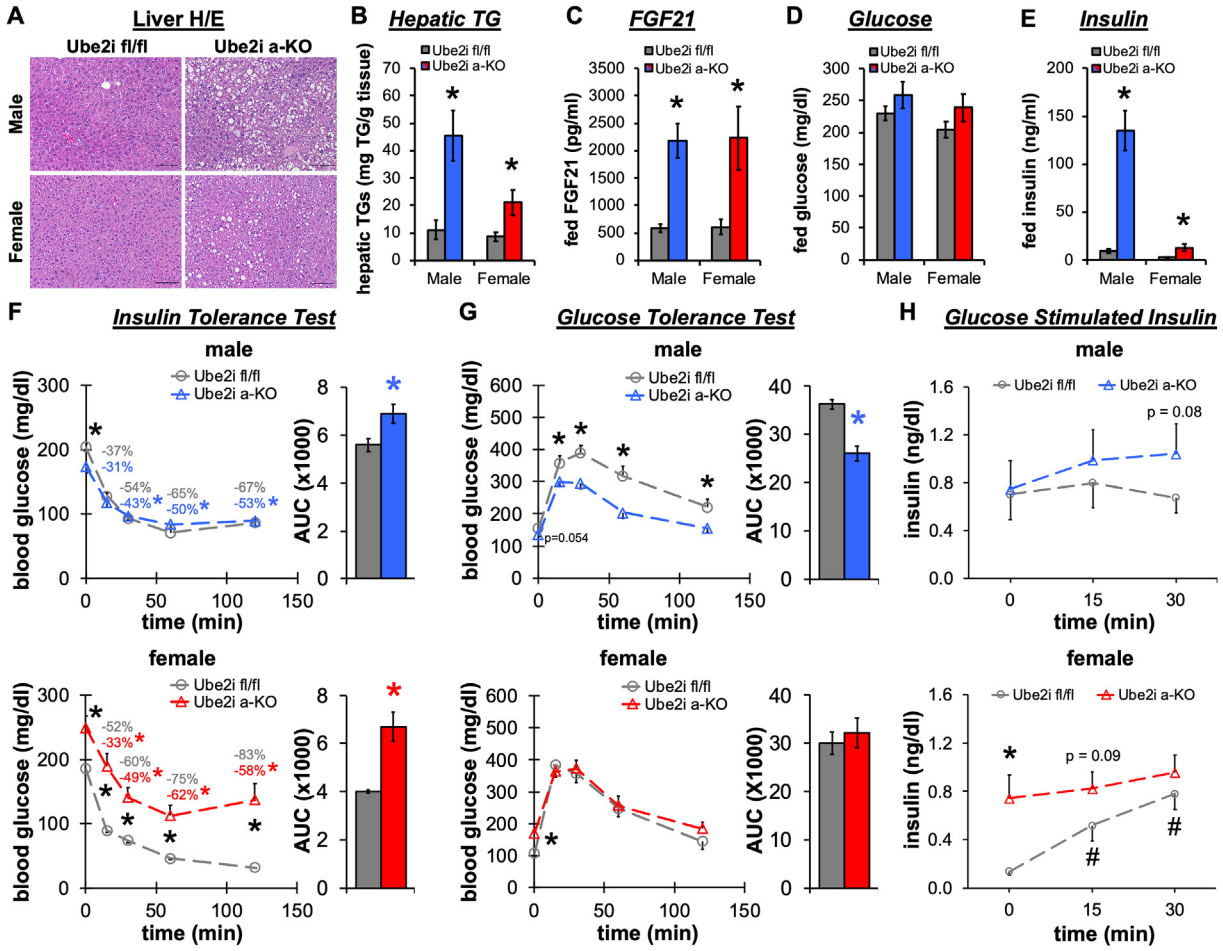

Figure 4: Adipocyte-specific *Ube2i* knockout mice develop insulin resistance and hepatic steatosis. **(A)** Representative H/E stained liver sections from male (top row) and female (bottom row) *Ube2i*$^{a\text{-}KO}$ and *Ube2i*$^{fl/fl}$ control mice show lipid droplet accumulation in *Ube2i*$^{a\text{-}KO}$ mice. Scale bar 100 μm. **(B)** Hepatic triglycerides (TGs) per gram liver tissue (n = 7/group). **(C)** Fed serum FGF21 (pg/ml) (male n = 11–12/group; female n = 7–9/group). **(D)** Fed serum glucose (mg/dl) and **(E)** insulin (ng/ml) (male n = 11–12/group; female n = 7–9/group). **(F)** Insulin and **(G)** glucose tolerances tests were performed on *Ube2i*$^{fl/fl}$ and *Ube2i*$^{a\text{-}KO}$ male (n = 11–15/group) and female (n = 5–7/group) mice. Area under the curve is also shown. Values labeled on panels in **(F)** indicate the percentage decrease from initial fasting blood glucose. **(H)** Serum insulin during glucose tolerance test from *Ube2i*$^{fl/fl}$ and *Ube2i*$^{a\text{-}KO}$ male (n = 5/group) and female (n = 4–6/group) mice. Gray = *Ube2i*$^{fl/fl}$ male and female controls, blue = male *Ube2i*$^{a\text{-}KO}$, red = female *Ube2i*$^{a\text{-}KO}$. Data are presented as mean +/− SEM; *p < 0.05 between groups, #p < 0.05 versus time zero. All analyses were performed in six-month-old adult mice.

and free fatty acids were significantly reduced in *Ube2i*$^{a\text{-}KO}$ mice compared to controls (Figure 3B). Adipocyte-specific deletion of *Ube2i* reduced hallmark adipocyte differentiation (*Adipoq*, *Pparγ2*, *Lep*, *Fabp4*), lipogenesis (*Fasn*, *Acaca*), and lipolysis (*Atgl*, *Lipe*) genes in WAT. Immune cell markers (*F4/80*, *Tnfa*, *Ifng*) and the collagen gene *Col1a1* were upregulated in both the gWAT and iWAT (Figure 3C), consistent with morphological changes. However, we noted divergent levels of inflammatory and lipogenesis genes in iWAT of males and females indicative of the known influence of sex on WAT [19]. Gene expression markers of senescence (*p16*) and the Nlrp3 inflammasome (*Il1b*, *Nlrp3*, *Pycard*, and *Casp1*) were particularly elevated in male WAT of *Ube2i*$^{a\text{-}KO}$, which may suggest increased innate and danger signal transduction in knockout mice. Indeed, we observed higher cleaved caspase-8 levels (Figure 3D) at six months of age, but not at one month, indicating increased cell death by apoptosis in *Ube2i*$^{a\text{-}KO}$ WAT and an important role for UBE2I in adipocyte survival of adolescent mice. Thus, impaired fat storage and WAT expansion in *Ube2i*$^{a\text{-}KO}$ mice coincides with inflammatory responses that drive adipocyte cell death.

3.4. Hepatosteatosis and insulin resistance in adult *Ube2i*$^{a\text{-}KO}$ mice

The inability of WAT depots to sequester lipids causes ectopic accumulation of energy in peripheral organs and lipodystrophic phenotypes [20]. Accordingly, six-month-old *Ube2i*$^{a\text{-}KO}$ mice developed fatty liver disease on a normal chow diet. Both male and female *Ube2i*$^{a\text{-}KO}$ mice displayed hepatic lipid droplet accumulation (Figure 4A) with significantly increased TG content (Figure 4B). FGF21 levels were increased 4-fold in *Ube2i*$^{a\text{-}KO}$ serum compared to controls (Figure 4C), indicating elevated stress responses in the liver [21]. *Ad libitum* fed glucose levels trended higher in *Ube2i*$^{a\text{-}KO}$ (Figure 4D), despite dramatically elevated levels of serum insulin (Figure 4E). Interestingly, we detected ~14-fold higher serum insulin levels in male *Ube2i*$^{a\text{-}KO}$ mice while females exhibited only a 4-fold increase compared to controls. To test the consequences of adipose tissue loss on glucose homeostasis, we performed insulin (Figure 4F) and glucose tolerance tests (Figure 4G). *Ube2i*$^{a\text{-}KO}$ male and female mice were insulin resistant relative to controls. However, with a prolonged fast, male *Ube2i*$^{a\text{-}KO}$ showed improved glucose intolerance with a lower fasting glucose level. Glucose stimulated insulin secretion during glucose tolerance tests in

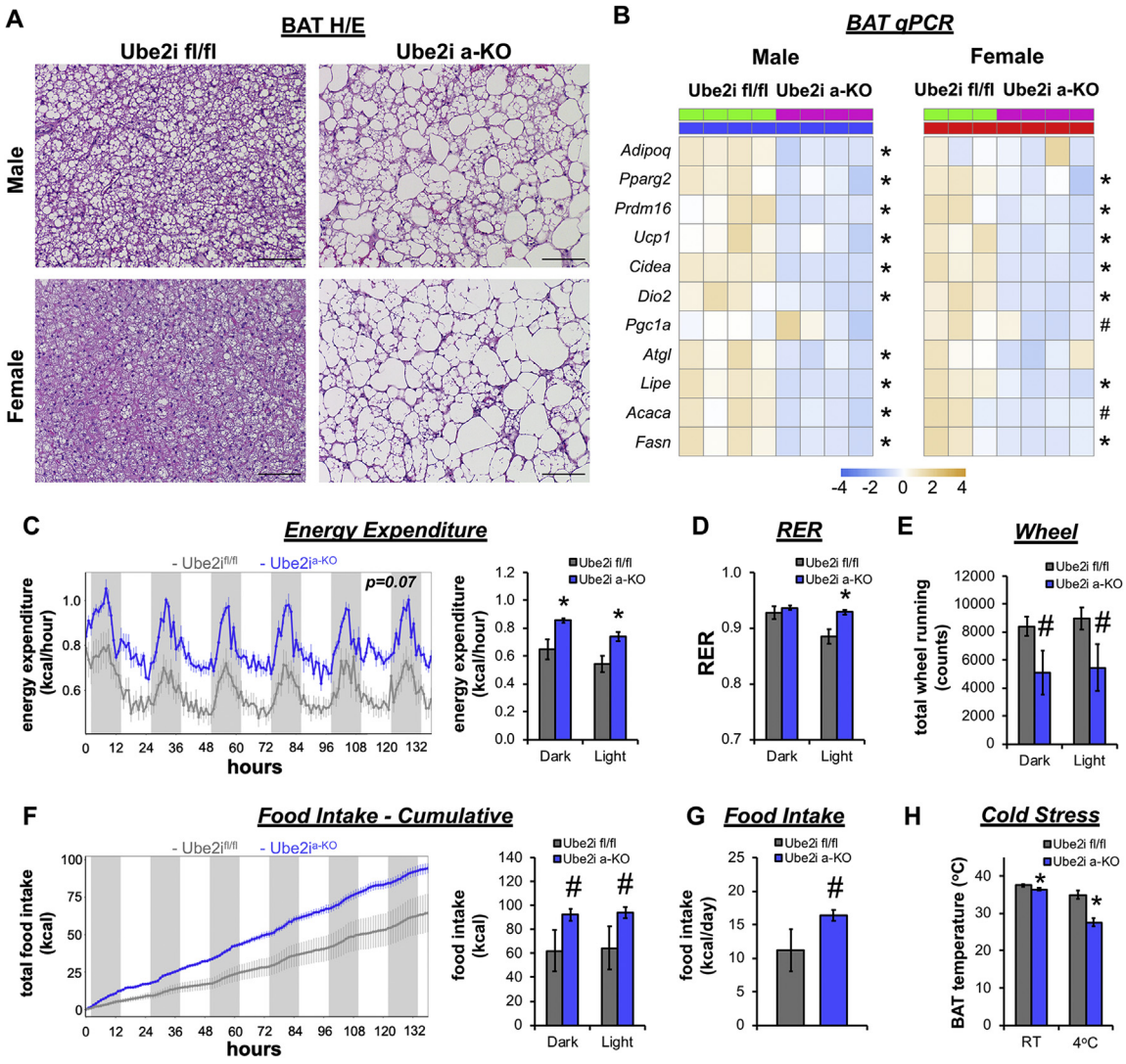

Figure 5: Adipocyte-specific *Ube2i* deletion increases energy expenditure and cold intolerance. (A) H/E stained BAT sections from male and female $Ube2i^{fl/fl}$ and $Ube2i^{a\text{-}KO}$ mice show large unilocular lipid droplets in $Ube2i^{a\text{-}KO}$ mice. Scale bar 100 μm. **(B)** Relative gene expression by qPCR in BAT from male (left, blue) and female (right, red) $Ube2i^{a\text{-}KO}$ (pink) and $Ube2i^{fl/fl}$ control (green) mice for brown adipocyte and lipid metabolism genes represented as a heatmap of z-scores (*p $<$ 0.05, #p $<$ 0.10). Six-month-old $Ube2i^{fl/fl}$ (gray) and $Ube2i^{a\text{-}KO}$ (blue) male mice were individually housed and monitored in CLAMS home cages for 6 days (n = 4–5/group). **(C)** Recorded traces of energy expenditure (kcal/hour) with mean values for dark/light periods (kcal/h). **(D)** Average RER during dark and light periods. **(E)** Activity was measured by wheel running. **(F)** Recorded traces of cumulative food intake (kcal) with mean values for dark/light periods (kcal) and **(G)** total food intake (kcal) per day. **(H)** Temperature probes were inserted under the skin to monitor intrascapular BAT temperature before (room temperature, RT) and after 2.5 h of cold (4 °C) exposure (n = 3–5/group). Statistical analysis of energy expenditure was performed by ANCOVA with lean body mass as a co-variate and cumulative food intake by standard ANOVA. Data are presented as mean +/− SEM; *p $<$ 0.05, #p $<$ 0.10.

male $Ube2i^{a\text{-}KO}$ mice trended higher than that in controls (Figure 4H), but importantly, demonstrated that the beta cell adapts properly during fasting compared to the fed state, as observed previously for other lipodystrophic mice [22]. Conversely, fasting glucose was elevated in female $Ube2i^{a\text{-}KO}$ compared to controls, with nominal effects on overall glucose tolerance due to enhanced glucose stimulated insulin secretion (Figure 4H). In summary, female $Ube2i^{a\text{-}KO}$ mice demonstrate fasting hyperglycemia and substantially impaired insulin sensitivity, in contrast to male $Ube2i^{a\text{-}KO}$ that demonstrate modest insulin resistance with improved glucose clearance during glucose tolerance tests. The sex discrepancy in glucose tolerance may be partly explained by greater skeletal muscle mass available for glucose disposal [23], as suggested by 35% more lean mass in male $Ube2i^{a\text{-}KO}$ than in female $Ube2i^{a\text{-}KO}$ mice (Figure 2F).

3.5. Adipocyte-specific *Ube2i* deletion increases energy expenditure

We subsequently investigated the effects of $Ube2i^{a\text{-}KO}$ on energy expenditure and BAT thermogenic functions. Histological assessment of H/E stained BAT sections from $Ube2i^{a\text{-}KO}$ male and female mice demonstrated lipid accumulation in large unilocular fat droplets, in contrast to the small multi-locular fat droplets characteristic of controls (Figure 5A). $Ube2i^{a\text{-}KO}$ caused dysfunctional BAT gene expression (Figure 5B) as reflected by reduced levels of hallmark brown adipocyte genes (*Prdm16*, *Ucp1*, *Cidea*, and *Dio2*) and key lipid metabolism genes (*Atgl*, *Lipe*, *Acaca*, and *Fasn*). Adult male $Ube2i^{a\text{-}KO}$ mice were placed in CLAMS home cages to assess heat production (energy expenditure) by indirect calorimetry. $Ube2i^{a\text{-}KO}$ mice exhibited increased energy expenditure (Figure 5C) and primarily used glucose

as a fuel source during the light period (Figure 5D) as indicated by an elevated respiratory exchange ratio (RER). Increased energy expenditure was not associated with higher activity levels (Figure 5E), but rather poor metabolic flexibility likely stimulated greater food intake (Figure 5F,G) and consequently elevated energy expenditure in *Ube2i*$^{a\text{-}KO}$ mice. To test the functional output of BAT, we performed a cold tolerance test in the absence of food. Before cold exposure, BAT temperature was reduced in *Ube2i*$^{a\text{-}KO}$ mice compared to controls and dramatically dropped after 2.5 h at 4 °C (Figure 5H), demonstrating an inability of *Ube2i*$^{a\text{-}KO}$ mice to defend body temperature. These experiments demonstrate that *Ube2i*$^{a\text{-}KO}$ causes a hypermetabolic phenotype coupled with metabolic inflexibility and BAT thermogenic defects. Collectively, adipocyte-specific deletion of *Ube2i* impairs WAT expansion fostering ectopic lipid accumulation in peripheral organs, compromising insulin sensitivity and thermogenesis.

4. DISCUSSION

Our previous work identified the E2 SUMO conjugating enzyme, *Ube2i*, as a negative regulator of fat cell differentiation in human subcutaneous preadipocytes [10]. In the present study, we generated adipocyte-specific *Ube2i* knockout (*Ube2i*$^{a\text{-}KO}$) mice to define the *in vivo* functions of *Ube2i* in mature fat cells. To our surprise, male and female *Ube2i*$^{a\text{-}KO}$ mice developed a hypermetabolic phenotype and progressive WAT lipoatrophy associated with immune cell infiltration and decreased circulating adipokines. *Ube2i*$^{a\text{-}KO}$ mice exhibited additional hallmark features of lipodystrophy, including ectopic lipid deposition in the liver, insulin resistance, and metabolic inflexibility. *Ube2i*$^{a\text{-}KO}$ WAT and BAT show broad dysfunction reflected by the expression of genes involved in energy storage and mobilization. These studies demonstrate previously unrealized functions of *Ube2i* in mouse WAT that are essential for mature adipocyte function and survival.

Patients with congenital general (CGL) or familial partial (FPLD) lipodystrophy exhibit profound insulin resistance, hepatic steatosis, and dyslipidemia. Female patients in particular develop more severe metabolic complications than males [24,25]. Similarly, impaired glucose and insulin tolerance in *Ube2i*$^{a\text{-}KO}$ mice were more pronounced in females, attributed in part to a greater skeletal muscle mass in male mice available for glucose disposal [23]. In terms of fat mass, CGL patients have extreme deficits at birth due to autosomal recessive mutations, while FPLD patients develop progressive fat loss beginning at puberty [2,24–26]. *Ube2i*$^{a\text{-}KO}$ mice resemble FPLD because WAT mass was normal in *Ube2i*$^{a\text{-}KO}$ mice after birth, but began to decrease during puberty, with as little as 2% remaining by six months. The timing of fat loss in *Ube2i*$^{a\text{-}KO}$ mice is consistent with a period of hypertrophic WAT expansion [27], impairments of which degrade adipocyte maturation and endocrine functions. Accordingly, inhibition of SUMOylation in differentiated cells [28] decreased adipocyte lipid storage and maturation genes (*Pparγ*, *C/ebpa*, *Fabp4*). Collectively, these observations suggest that *Ube2i* has a distinct role in adult adipocyte function, maturation, and survival.

A few lipodystrophic mouse models develop progressive lipoatrophy and hepatic steatosis, such as adipocyte-specific knockout of Akt1/Akt2 [29], insulin receptor [30], Raptor [31], and PPARγ [4]. Our model has many features similar to those of progressive lipoatrophy observed in PPARγ knockout models [4,8]. Lipoatrophy in fat-specific PPARγ knockout mice occurs because adipocytes lost lipids and shrank, consistent with the pivotal roles of PPARγ as a master regulator of adipose tissue formation [4,32]. PPARγ ablation in Sox2-expressing cells (PPARγ$^{\Delta/\Delta}$) skirts embryonic lethality and mice survive without WAT and BAT [8]. PPARγ$^{\Delta/\Delta}$ show a hypermetabolic phenotype accompanied by higher energy expenditure and hyperphagia. Similar to *Ube2i*$^{a\text{-}KO}$ mice, PPARγ$^{\Delta/\Delta}$ mice show higher RER and glucose oxidation that derives from more lean mass. Alternatively, depletion of circulating leptin in lipoatrophy would increase hyperphagia and could underlie hyperinsulinemia and increased energy expenditure. However, at least one model demonstrated that increased food intake was independent of leptin levels in lipoatrophic mice [33]. The liver dominates mass-specific metabolic rates [34] and, consequently, the hepatomegaly and hyperinsulinemia present in *Ube2i*$^{a\text{-}KO}$ likely contribute to greater glucose oxidation and metabolic inflexibility. Elevated energy expenditure and metabolic defects are similarly observed in other lipodystrophic mouse models [8,35,36]. Our observations expand on these studies and document a putative role for *Ube2i* and PPARγ interactions [10] in maintaining adipose tissue homeostasis during postnatal growth.

For reasons that remain unclear, *Ube2i* expression peaks early in differentiation of 3T3-L1 adipocytes, when adiponectin remains low, to regulate expression of the key adipogenic transcription factors PPARγ, C/EBPα, and C/EBPβ [37]. Adiponectin expression occurs late in adipogenesis [38] and Adipoq-Cre mediated ablation of *Ube2i* occurs in relatively mature adipocytes. While impaired adipogenesis underlies the development of lipodystrophy in some models [8,35,36,39], it is unlikely to account for lipoatrophy in *Ube2i*$^{a\text{-}KO}$ mice. The more dramatic lipodystrophy in older *Ube2i*$^{a\text{-}KO}$ mice likely results from apoptosis and inflammation, consistent with the pivotal roles of *Ube2i* in cell survival across many tissue types [14]. Cell survival also depends on preservation of the nuclear architecture, evident by the embryonic lethality of *Ube2i* deficiency [16]. Additionally, *Ube2i* occupies transcriptional start sites of functional genes integral for cell growth and proliferation [40]. However, loss of *Ube2i* induces cell growth arrest, due in part, to impaired chromosome segregation, which contributes to reduced cell viability [40]. Along these lines, the lipoatrophy caused by induction of caspase 8 in Fabp4-positive adipocytes [33] mirrors some features of *Ube2i*$^{a\text{-}KO}$ mice, including WAT inflammation and depletion of adipokines. However, recombination of alleles in other Fabp4-positive adipocytes and other tissues [41] likely contributes to some of the metabolic phenotype upon caspase-8 induction. Of note, the expression of NLRP3 inflammasome genes (*Nlrp3*, *Il-1b*, *Pycard*, *Casp1*) correlate with elevated cleaved Caspase-8 in WAT of *Ube2i*$^{a\text{-}KO}$, suggesting a potential mechanism [42] for adipocyte cell death. New studies that use temporal deletion strategies [27] will provide insight into whether acute deletion of *Ube2i* in adult mice causes lipodystrophy from fat cell death or restricted adipocyte turnover.

Ube2i exerts a diverse array of cellular functions through SUMOylation and protein–protein interactions that influence gene transcription among many others roles [43]. During adipocyte differentiation, *Ube2i* knockdown de-represses transcription of the brown fat gene program, enabling the master transcription factor PPARγ to bind to UCP1 enhancers promoting uncoupled respiration [10]. Moreover, *Ube2i* interacts with the master transcription factor PPARγ to suppress DNA occupancy and ligand dependent activity *in vitro* [10]. *In vivo*, mice resistant to PPARγ SUMOylation at K107 exhibit better insulin sensitivity [44]. In some settings, SUMOylation prevents ubiquitination and protein turnover. For example, Cbx4 serves as SUMO E3 ligase that stabilizes PRDM16 to facilitate thermogenesis and glucose homeostasis [45], which may explain, at least in part, the cold intolerance and metabolic defects in *Ube2i*$^{a\text{-}KO}$ mice.

We and others demonstrated that SUMOylation of PPARγ broadly inhibits metabolic functions of white adipocytes [10,44,46]. Based on

these data, we predicted greater beige fat thermogenesis and improved energy balance in *Ube2i*$^{a\text{-}KO}$ mice relative to littermate controls. The lack of exact agreement between phenotypes observed in tissue culture versus whole animals is not surprising, but perhaps expected due to the importance of *Ube2i* in cell survival [14,16]. *Ube2i* knockout in adipocytes may also cause depletion of adipocyte progenitor cells coupled with Ucp1 deregulation and induction of the fibro-inflammatory program seen in settings of accelerating ageing [47]. Regardless, the extensive roles of *Ube2i* suggest the mechanism underlying lipoatrophy in *Ube2i*$^{a\text{-}KO}$ is unlikely to be the result of a single SUMOylation event. It will now be important to use mass spectrometry and lineage tracing methods to identify the most critical metabolic and transcription factors downstream of *Ube2i* functions that explain why *Ube2i* allows WAT expansion during ageing.

Conditions of lipodystrophy and pathologic obesity suffer from a restricted capacity to expand white adipose depots to meet the demand for nutrient storage, which drives adipocyte dysfunction and WAT inflammation, along with ectopic lipid accumulation and insulin resistance [48]. Ultimately, identifying factors that enable healthy WAT expansion carries significant implications for treating diseases associated with fat storage and metabolism, including obesity and lipodystrophy. The striking phenotype of *Ube2i*$^{a\text{-}KO}$ mice reveals the cell-autonomous necessity of *Ube2i* in healthy adipose tissue maintenance and whole-body energy balance. As a rate-limiting E2 SUMO conjugating enzyme necessary for SUMOylation, this mouse model provides a valuable tool for understanding how the low-abundance post-translational modification SUMOylation [49] broadly affects mature adipocyte function and, more broadly, tissue development. In addition, *Ube2i*$^{a\text{-}KO}$ mice add to a small list of mouse models to study systemic effects of WAT loss during postnatal development and fundamental aspects of energy balance.

FUNDING

This work was funded by American Diabetes Association #1-18-IBS-105, and NIH R01DK 126042, R01DK114356 (to S.M.H.), R01 DK111436 (to Z.S.), R01 HD085994 and T32 HD098068 (to S.A.P). This study was also funded (in part) by an award from the Baylor College of Medicine Nutrition and Obesity Pilot and Feasibility Fund (to A.R.C.) and the Nancy Chang, PhD Award for Research Excellence at BCM (to S.M.H.). This study was also supported by the Assistant Secretary of Defense for Health Affairs endorsed by the DOD PRMRP Discovery Award (No. W81XWH-18-1-0126 to K.H.K.). Core services at BCM utilized in this project were supported with funding from NCI P30-CA125123: Genetically Engineered Rodent Models Core, Human Tissue Acquisition and Histology Core, and the Integrated Microscopy Core.

AUTHOR CONTRIBUTIONS

A.R.C. and S.M.H. conceptualized the study. P.M., N.C., A.R.C., and S.M.H. designed the experiments. A.R.C. and S.M.H. wrote the manuscript with editorial input from all authors. S.M.H. and A.R.C performed all experiments with assistance as noted: P.K.S. assisted with mouse phenotyping; A.R.C. performed qPCR analysis with assistance from J.B.F., N.C. and R.S.; D.D.M., S.M.B., and S.A.P. performed genotyping and troubleshooting; K.H.K. performed analysis of liver lipids. X.L. and Z.S. provided resources and support for body temperature experiments. All work was performed under the supervision of S.M.H. The authors thank Robb Moses (BCM) for reading drafts of the manuscript.

CONFLICT OF INTEREST

None declared.

APPENDIX A. SUPPLEMENTARY DATA

Supplementary data to this article can be found online at https://doi.org/10.1016/j.molmet.2021.101221.

REFERENCES

[1] Roden, M., Shulman, G.I., 2019. The integrative biology of type 2 diabetes. Nature 576(7785):51—60.
[2] Garg, A., 2004. Acquired and inherited lipodystrophies. New England Journal of Medicine 350(12):1220—1234.
[3] Cristancho, A.G., Lazar, M.A., 2011. Forming functional fat: a growing understanding of adipocyte differentiation. Nature Reviews Molecular Cell Biology 12(11):722—734.
[4] Wang, F., Mullican, S.E., DiSpirito, J.R., Peed, L.C., Lazar, M.A., 2013. Lipoatrophy and severe metabolic disturbance in mice with fat-specific deletion of PPARγ. Proceedings of the National Academy of Sciences of the United States of America 110(46):18656—18661.
[5] Rajakumari, S., Wu, J., Ishibashi, J., Lim, H.-W., Giang, A.-H., Won, K.-J., et al., 2013. EBF2 determines and maintains brown adipocyte identity. Cell Metabolism 17(4):562—574.
[6] Seale, P., Bjork, B., Yang, W., Kajimura, S., Chin, S., Kuang, S., et al., 2008. PRDM16 controls a brown fat/skeletal muscle switch. Nature 454(7207):961—967.
[7] Barak, Y., Nelson, M.C., Ong, E.S., Jones, Y.Z., Ruiz-Lozano, P., Chien, K.R., et al., 1999. PPAR gamma is required for placental, cardiac, and adipose tissue development. Molecular Cell 4(4):585—595.
[8] Gilardi, F., Winkler, C., Quignodon, L., Diserens, J.G., Toffoli, B., Schiffrin, M., et al., 2019. Systemic PPARγ deletion in mice provokes lipoatrophy, organomegaly, severe type 2 diabetes and metabolic inflexibility. Metabolism 95: 8—20.
[9] Rosen, E.D., Sarraf, P., Troy, A.E., Bradwin, G., Moore, K., Milstone, D.S., et al., 1999. PPAR gamma is required for the differentiation of adipose tissue in vivo and in vitro. Molecular Cell 4(4):611—617.
[10] Hartig, S.M., Bader, D.A., Abadie, K.V., Motamed, M., Hamilton, M.P., Long, W., et al., 2015. Ubc9 impairs activation of the brown fat energy metabolism program in human white adipocytes. Molecular Endocrinology 29(9):1320—1333.
[11] Lanza, D.G., Gaspero, A., Lorenzo, I., Liao, L., Zheng, P., Wang, Y., et al., 2018. Comparative analysis of single-stranded DNA donors to generate conditional null mouse alleles. BMC Biology 16(1):69.
[12] Mina, A.I., LeClair, R.A., LeClair, K.B., Cohen, D.E., Lantier, L., Banks, A.S., 2018. CalR: a web-based analysis tool for indirect calorimetry experiments. Cell Metabolism 28(4):656—666 e651.
[13] Koh, E.H., Chernis, N., Saha, P.K., Xiao, L., Bader, D.A., Zhu, B., et al., 2018. miR-30a remodels subcutaneous adipose tissue inflammation to improve insulin sensitivity in obesity. Diabetes 67(12):2541—2553.
[14] Demarque, M.D., Nacerddine, K., Neyret-Kahn, H., Andrieux, A., Danenberg, E., Jouvion, G., et al., 2011. Sumoylation by Ubc9 regulates the stem cell compartment and structure and function of the intestinal epithelium in mice. Gastroenterology 140(1):286—296.
[15] Ding, X., Wang, A., Ma, X., Demarque, M., Jin, W., Xin, H., et al., 2016. Protein SUMOylation is required for regulatory T cell expansion and function. Cell Reports 16(4):1055—1066.
[16] Nacerddine, K., Lehembre, F., Bhaumik, M., Artus, J., Cohen-Tannoudji, M., Babinet, C., et al., 2005. The SUMO pathway is essential for nuclear integrity and chromosome segregation in mice. Developmental Cell 9(6):769—779.

[17] Rodriguez, A., Briley, S.M., Patton, B.K., Tripurani, S.K., Rajapakshe, K., Coarfa, C., et al., 2019. Loss of the E2 SUMO-conjugating enzyme Ube2i in oocytes during ovarian folliculogenesis causes infertility in mice. Development 146(23).

[18] Murano, I., Barbatelli, G., Parisani, V., Latini, C., Muzzonigro, G., Castellucci, M., et al., 2008. Dead adipocytes, detected as crown-like structures, are prevalent in visceral fat depots of genetically obese mice. The Journal of Lipid Research 49(7):1562–1568.

[19] Goossens, G.H., Jocken, J.W.E., Blaak, E.E., 2021. Sexual dimorphism in cardiometabolic health: the role of adipose tissue, muscle and liver. Nature Reviews Endocrinology 17(1):47–66.

[20] Savage, D.B., Murgatroyd, P.R., Chatterjee, V.K., O'Rahilly, S., 2005. Energy expenditure and adaptive responses to an acute hypercaloric fat load in humans with lipodystrophy. Journal of Clinical Endocrinology & Metabolism 90(3):1446–1452.

[21] Fisher, F.M., Maratos-Flier, E., 2016. Understanding the physiology of FGF21. Annual Review of Physiology 78:223–241.

[22] Moitra, J., Mason, M.M., Olive, M., Krylov, D., Gavrilova, O., Marcus-Samuels, B., et al., 1998. Life without white fat: a transgenic mouse. Genes & Development 12(20):3168–3181.

[23] Xu, W., Zhou, H., Xuan, H., Saha, P., Wang, G., Chen, W., 2019. Novel metabolic disorders in skeletal muscle of Lipodystrophic Bscl2/Seipin deficient mice. Molecular and Cellular Endocrinology 482:1–10.

[24] Araújo-Vilar, D., Loidi, L., Domínguez, F., Cabezas-Cerrato, J., 2003. Phenotypic gender differences in subjects with familial partial lipodystrophy (Dunnigan variety) due to a nuclear lamin A/C R482W mutation. Hormone and Metabolic Research 35(1):29–35.

[25] Van Maldergem, L., Magré, J., Khallouf, T.E., Gedde-Dahl, T., Delépine, M., Trygstad, O., et al., 2002. Genotype-phenotype relationships in Berardinelli-Seip congenital lipodystrophy. Journal of Medical Genetics 39(10):722–733.

[26] Dunnigan, M.G., Cochrane, M.A., Kelly, A., Scott, J.W., 1974. Familial lipoatrophic diabetes with dominant transmission. A new syndrome. Quarterly Journal of Medicine 43(169):33–48.

[27] Wang, Q.A., Tao, C., Gupta, R.K., Scherer, P.E., 2013. Tracking adipogenesis during white adipose tissue development, expansion and regeneration. Nature Medicine 19(10):1338–1344.

[28] Liu, H., Li, J., Lu, D., Li, J., Liu, M., He, Y., et al., 2018. Ginkgolic acid, a sumoylation inhibitor, promotes adipocyte commitment but suppresses adipocyte terminal differentiation of mouse bone marrow stromal cells. Scientific Reports 8(1):2545.

[29] Shearin, A.L., Monks, B.R., Seale, P., Birnbaum, M.J., 2016. Lack of AKT in adipocytes causes severe lipodystrophy. Molecular Metabolism 5(7):472–479.

[30] Softic, S., Boucher, J., Solheim, M.H., Fujisaka, S., Haering, M.F., Homan, E.P., et al., 2016. Lipodystrophy due to adipose tissue-specific insulin receptor knockout results in progressive NAFLD. Diabetes 65(8):2187–2200.

[31] Lee, P.L., Tang, Y., Li, H., Guertin, D.A., 2016. Raptor/mTORC1 loss in adipocytes causes progressive lipodystrophy and fatty liver disease. Molecular Metabolism 5(6):422–432.

[32] He, W., Barak, Y., Hevener, A., Olson, P., Liao, D., Le, J., et al., 2003. Adipose-specific peroxisome proliferator-activated receptor gamma knockout causes insulin resistance in fat and liver but not in muscle. Proceedings of the National Academy of Sciences of the United States of America 100(26):15712–15717.

[33] Pajvani, U.B., Trujillo, M.E., Combs, T.P., Iyengar, P., Jelicks, L., Roth, K.A., et al., 2005. Fat apoptosis through targeted activation of caspase 8: a new mouse model of inducible and reversible lipoatrophy. Nature Medicine 11(7):797–803.

[34] Rolfe, D.F., Brown, G.C., 1997. Cellular energy utilization and molecular origin of standard metabolic rate in mammals. Physiological Reviews 77(3):731–758.

[35] Péterfy, M., Phan, J., Xu, P., Reue, K., 2001. Lipodystrophy in the fld mouse results from mutation of a new gene encoding a nuclear protein, lipin. Nature Genetics 27(1):121–124.

[36] Cortés, V.A., Curtis, D.E., Sukumaran, S., Shao, X., Parameswara, V., Rashid, S., et al., 2009. Molecular mechanisms of hepatic steatosis and insulin resistance in the AGPAT2-deficient mouse model of congenital generalized lipodystrophy. Cell Metabolism 9(2):165–176.

[37] Cignarelli, A., Melchiorre, M., Peschechera, A., Conserva, A., Renna, L.A., Miccoli, S., et al., 2010. Role of UBC9 in the regulation of the adipogenic program in 3T3-L1 adipocytes. Endocrinology 151(11):5255–5266.

[38] Hu, E., Liang, P., Spiegelman, B.M., 1996. AdipoQ is a novel adipose-specific gene dysregulated in obesity. Journal of Biological Chemistry 271(18):10697–10703.

[39] Chen, W., Chang, B., Saha, P., Hartig, S.M., Li, L., Reddy, V.T., et al., 2012. Berardinelli-seip congenital lipodystrophy 2/seipin is a cell-autonomous regulator of lipolysis essential for adipocyte differentiation. Molecular and Cellular Biology 32(6):1099–1111.

[40] Neyret-Kahn, H., Benhamed, M., Ye, T., Le Gras, S., Cossec, J.-C., Lapaquette, P., et al., 2013. Sumoylation at chromatin governs coordinated repression of a transcriptional program essential for cell growth and proliferation. Genome Research 23(10):1563–1579.

[41] Lee, K.Y., Russell, S.J., Ussar, S., Boucher, J., Vernochet, C., Mori, M.A., et al., 2013. Lessons on conditional gene targeting in mouse adipose tissue. Diabetes 62(3):864–874.

[42] Giordano, A., Murano, I., Mondini, E., Perugini, J., Smorlesi, A., Severi, I., et al., 2013. Obese adipocytes show ultrastructural features of stressed cells and die of pyroptosis. The Journal of Lipid Research 54(9):2423–2436.

[43] Chang, H.M., Yeh, E.T.H., 2020. SUMO: from bench to bedside. Physiological Reviews 100(4):1599–1619.

[44] Katafuchi, T., Holland, W.L., Kollipara, R.K., Kittler, R., Mangelsdorf, D.J., Kliewer, S.A., 2018. PPARγ-K107 SUMOylation regulates insulin sensitivity but not adiposity in mice. Proceedings of the National Academy of Sciences of the United States of America 115(48):12102–12111.

[45] Chen, Q., Huang, L., Pan, D., Zhu, L.J., Wang, Y.X., 2018. Cbx4 sumoylates Prdm16 to regulate adipose tissue thermogenesis. Cell Reports 22(11):2860–2872.

[46] Dutchak, P.A., Katafuchi, T., Bookout, A.L., Choi, J.H., Yu, R.T., Mangelsdorf, D.J., et al., 2012. Fibroblast growth factor-21 regulates PPARγ activity and the antidiabetic actions of thiazolidinediones. Cell 148(3):556–567.

[47] Gao, Z., Daquinag, A.C., Fussell, C., Zhao, Z., Dai, Y., Rivera, A., et al., 2020. Age-associated telomere attrition in adipocyte progenitors predisposes to metabolic disease. Nature Metabolism 2(12):1482–1497.

[48] Kahn, C.R., Wang, G., Lee, K.Y., 2019. Altered adipose tissue and adipocyte function in the pathogenesis of metabolic syndrome. Journal of Clinical Investigation 129(10):3990–4000.

[49] Lamoliatte, F., Caron, D., Durette, C., Mahrouche, L., Maroui, M.A., Caron-Lizotte, O., et al., 2014. Large-scale analysis of lysine SUMOylation by SUMO remnant immunoaffinity profiling. Nature Communications 5:5409.

